Lagrangian Transport by Nonbreaking and Breaking Deep-Water Waves at the Ocean Surface

NICK PIZZO AND W. KENDALL MELVILLE

Scripps Institution of Oceanography, University of California, San Diego, La Jolla, California

LUC DEIKE

Department of Mechanical and Aerospace Engineering, Princeton University Princeton Environmental Institute, Princeton University, Princeton, New Jersey

(Manuscript received 31 October 2018, in final form 2 February 2019)

ABSTRACT

Using direct numerical simulations (DNS), Deike et al. found that the wave-breaking-induced mass transport, or drift, at the surface for a single breaking wave scales linearly with the slope of a focusing wave packet, and may be up to an order of magnitude larger than the prediction of the classical Stokes drift. This model for the drift due to an individual breaking wave, together with the statistics of wave breaking measured in the field, are used to compute the Lagrangian drift of breaking waves in the ocean. It is found that breaking may contribute up to an additional 30% to the predicted values of the classical Stokes drift of the wave field for the field experiments considered here, which have wind speeds ranging from 1.6 to 16 m s^{-1}, significant wave heights in the range of 0.7–4.7 m, and wave ages (defined here as c_m/u_*, for the spectrally weighted phase velocity c_m and the wind friction velocity u_*) ranging from 16 to 150. The drift induced by wave breaking becomes increasingly more important with increasing wind friction velocity and increasing significant wave height.

1. Introduction

Lagrangian drift at the ocean surface plays a fundamental role in the kinematics and dynamics of the surface layers of the ocean. In the case of Langmuir circulations, their generation and evolution comes about primarily from Kelvin's circulation theorem and the vorticity of the wind-driven current. Furthermore, there are significant practical applications in predicting the transport of flotsam, jetsam, and pollution at the surface. The standard approach to this problem is to combine the classical Stokes drift due to linear irrotational surface waves (Kenyon 1969) with estimates of the wind drift, often based on laboratory experiments correlated with the wind friction velocity u_* (Wu 1975, 1982; Mueller and Veron 2009). An accurate representation of upper-ocean processes such as Langmuir circulations, and momentum transfer from the atmosphere to the water column, is therefore dependent on a correct representation of the wave-induced drift (McWilliams and Restrepo 1999). However, as far as we are aware no account has been made of the contribution of surface wave breaking to the surface drift, or surface current, a particularly significant contribution since under most conditions wave breaking is an important contributor to the generation of ocean currents (Terray et al. 1996; Melville et al. 1998; Donelan 1998; Veron and Melville 2001; Banner and Peirson 2007; Sullivan et al. 2004, 2007; Cavaleri et al. 2012; Pizzo and Melville 2013; Pizzo et al. 2016).

Using direct numerical simulations (DNS) of focusing wave packets and a scaling argument based on John's equation (John 1953; Pizzo 2017), Deike et al. (2017b) showed that prior to breaking the wave-induced Lagrangian drift was consistent with the classical theory, being proportional to a measure of the wave slope squared; however, with the onset of breaking the horizontal Lagrangian drift averaged over a wavelength around the breaking region was proportional to a measure of the slope of the packet. This is shown in Fig. 1a, where a particle that is transported by a nonbreaking wave is shown in the top panel, while a particle that is transported due to breaking is shown in the bottom

Corresponding author: Nick Pizzo, npizzo@ucsd.edu

DOI: 10.1175/JPO-D-18-0227.1

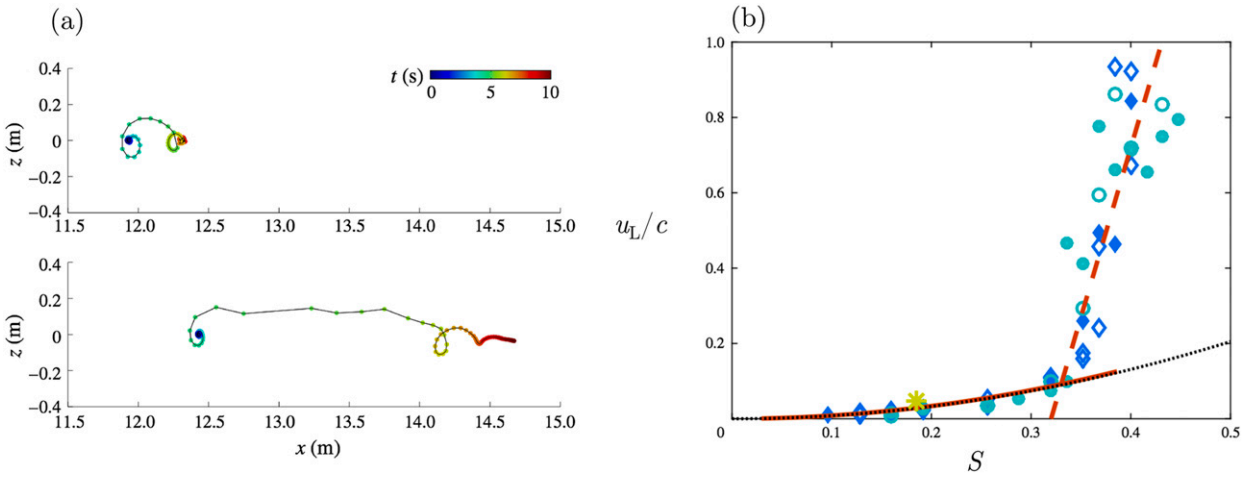

FIG. 1. (a) Particle trajectories in a (top) nonbreaking and (bottom) breaking deep-water surface wave, from the DNS of Deike et al. (2017b). Particles travel much further in the case of a breaking wave. Note, the particles are always in the water in these cases, never leaving it as spray. (b) For particles originally at the surface, the normalized Lagrangian drift induced by waves u_L/c, where c is a characteristic phase speed, as a function of the linear prediction of the maximum slope at focusing S, a measure of the strength of breaking for $S > S_0$, for S_0 a breaking threshold found here to be 0.31. For $S < S_0$, the waves do not break and the drift is well described by the classical theory of Stokes drift, which predicts the drift grows quadratically with S. For $S > S_0$ the waves break, and the drift grows linearly with S and is described by the model proposed by Deike et al. (2017b), shown by the dashed line. Diamonds and circles are DNS data from Deike et al. (2017b), while the star is an experimental measurement from Grue and Kolaas (2017).

panel. Note, the mass transport for nonbreaking wave packets have been studied recently by van den Bremer and Taylor (2016) and van den Bremer and Breivik (2018). The particle transported due to breaking travels nearly an order of magnitude further than the particle in the nonbreaking case. This increase is quantified in Fig. 1b, where drift speeds up to an order of magnitude larger than the classical predictions are observed for strong breaking waves.

In this paper we take these new results based on the DNS and theoretical scaling and apply similar techniques to those that we have used in the past to extend results from DNS, theory and the laboratory to the ocean using field measurements of Phillips's (1985) breaking statistic $\Lambda(\mathbf{c})d\mathbf{c}$ (Kleiss and Melville 2010; Zappa et al. 2012; Sutherland and Melville 2013; Schwendeman et al. 2014; Sutherland and Melville 2015), the average length of breaking crests moving with velocities in the range $(\mathbf{c}, \mathbf{c} + d\mathbf{c})$ per unit area of ocean surface. In the past these have included momentum flux and wave dissipation (Romero et al. 2012; Sutherland and Melville 2013, 2015), air entrainment (Deike et al. 2017a), and gas transfer (Deike and Melville 2018). In this case we are predicting the contribution of Lagrangian drift due to breaking to the total Lagrangian drift due to waves at the ocean surface.

The environmental conditions considered here have wind speeds ranging from 1.6 to 16 m s^{-1}, significant wave heights in the range of 0.7–4.7 m and wave ages [defined as c_m/u_*, for c_m the spectrally weighted phase velocity of the wind-wave spectrum (which is found to scale linearly with the phase speed of the spectral peak c_p and is a better integral characterization of the wind-wave spectrum, as opposed to c_p, which is often representative of the swell) following Sutherland and Melville (2015), and u_* is the wind friction velocity] ranging from 16 to 150. Note, wave breaking is more common in young seas and predominantly occurs in the wind-wave portion of the wave spectrum (Sutherland and Melville 2013). It should furthermore be mentioned explicitly that there are other sources of mass transport at the ocean surface, including large scale geostrophic flows, buoyancy driven transport, as well as the wind drift. Here, we are specifically focusing on the role of the surface wave field in transporting mass at the ocean surface.

Typically, water waves enter the larger scale (averaged over the fast time scales of the surface waves) equations of motion through the Stokes drift, and specifically in the vortex force term (see, e.g., McWilliams and Restrepo 1999; Suzuki and Fox-Kemper 2016). This has been used to provide a rational model for Langmuir circulation (Craik and Leibovich 1976). Breaking represents a transition from the largely irrotational surface wave field to vortical flow (Pizzo and Melville 2013; Pizzo et al. 2016), which has dynamical significance for the resulting kinematics and dynamics of the flow. This is illustrated in the LES simulations of Sullivan et al. (2007; see also Sullivan et al. 2004), where a body force model for breaking is used to examine its effects on the dynamics and statistics of the upper-ocean boundary

layer. Significant differences between scenarios with and without wave breaking are found. In terms of the mechanics of the upper-ocean boundary layer, wave breaking greatly enhances energy dissipation (and leads to large departures from law of the wall scaling; Melville 1994; Sutherland and Melville 2015), seeds the so-called CL2 mechanism (Leibovich 1983; Sullivan et al. 2004) by introducing vorticity into the water column, and modulates the transfer of mass, momentum, and energy between the water column, the wave field, and the atmosphere. Therefore, it is believed that properly resolving dynamical and integral properties of the breaking-induced flow will serve to better constrain budgets of mass, momentum, and energy in LES models of the air–sea boundary layer.

2. Wave-induced Lagrangian drift

In this section we review and derive models for the drift induced by nonbreaking and breaking deep water surface waves. Integrals of these quantities are presented, as are the values of integrands associated with these measures. Scaling arguments for these quantities are then discussed.

a. Classical Stokes drift

The classical Stokes drift is a result of the fact that the orbits of the elements of fluid in the irrotational surface waves are not closed but open leading to a slow drift motion. For a monochromatic deep-water irrotational wave field of amplitude a, wavenumber k, and frequency $\omega = \sqrt{gk}$, where g is the gravitational acceleration, the Stokes drift is given by

$$u_s = (ak)^2 c e^{2kz}, \tag{1}$$

where c is the phase speed and $z = 0$ is the undisturbed surface. For a directional spectrum of linear irrotational deep-water surface gravity waves defined by

$$\langle \eta^2 \rangle = \iint F(\mathbf{k})\, d\mathbf{k}, \tag{2}$$

where η is the surface displacement, $F(\mathbf{k})$ is the directional wave spectrum, and angle brackets denote averaging, the Stokes drift is given by Kenyon (1969) as

$$\mathbf{U}_S = 2\iint F(\mathbf{k})\sqrt{gk}e^{2kz}\mathbf{k}\, d\mathbf{k}, \tag{3}$$

where $k = |\mathbf{k}|$.

Although the variables of interest in this section are in general vector valued quantities, throughout the rest of this work we assume that the induced drift from nonbreaking and breaking waves aligns with the wind. A full discussion of the relative angles of these two phenomenon, while technically possible with measurements of the directional wave spectra and breaking statistics (Romero and Melville 2010; Lenain and Melville 2017), is outside the scope of this paper. We focus on the analysis of the angle-integrated data, in order to derive and test robust scaling laws. It follows that the azimuth-integrated Stokes drift at the surface (here taken to be at $z = 0$ for linear waves) can then be written as

$$U_S = 2\int \phi(k)\sqrt{gk}k\, dk, \tag{4}$$

where $\phi(k) = \int kF(\mathbf{k})\, d\theta = \int kF(k, \theta)\, d\theta$ is the azimuth integrated wave spectrum.

b. Lagrangian drift due to breaking

In the recent paper by Deike et al. (2017b) it was shown by DNS, supported by scaling based on John's equation (John 1953; Pizzo 2017), that when a focusing wave packet led to breaking the average Lagrangian drift of elements of fluid directly influenced by the breaking over a characteristic wavelength around the breaking front takes the form

$$u_{\mathrm{LB}} = \alpha(\mathscr{S} - \mathscr{S}_0)c, \tag{5}$$

where $\alpha = 9$ is a constant found by a best fit to the DNS data, $\mathscr{S}$ is a characteristic slope of the wave packet, $\mathscr{S}_0$ is a threshold slope for breaking, and $c(k)$ is the characteristic linear phase speed. Note, Rapp and Melville (1990) found that the depth of penetration of fluid due to breaking scales with the height of the wave at breaking, which is consistent with the scaling found in Deike et al. (2017b). This implies that there is still significant horizontal mass transport due to breaking up to a significant wave height down in the fluid, the e-folding scale for the breaking-induced drift being the breaking wave height, with approximately 50% of the surface drift at 1/2 a significant wave height, and approximately 10% of the surface breaking drift at 1/2 a wavelength. However, a complete understanding of the depth dependence of the breaking-induced drift under a complex wave spectrum remains to be understood, so in the remainder of this manuscript we examine the properties of the transport at the surface.

The scaling model described by Eq. (5) was derived based on the high-resolution DNS in Deike et al. (2017b). The fit of this model, at the surface ($z = 0$), with the available data is shown in Fig. 1b. These values are found by considering the total particle displacement for an ensemble of particles that are initially on the free surface and within a characteristic wavelength of the breaking location (taken to be the location where the free surface first becomes multivalued). These total

displacements are then averaged over the ensemble of particles, while the duration of breaking is assumed to scale with the characteristic period of the wave group (Rapp and Melville 1990; see discussion below), yielding a bulk scale measure of the mean transport speed of the broken fluid at the surface.

It follows that if $c\mathscr{T}\Lambda(c)dc$, for the duration $\mathscr{T}$ of the breaking event [and we recall that the breaking statistic $\Lambda(c)dc$ is the average length of breaking crests moving with velocity in the range $(c, c + dc)$ per unit area of ocean surface], is the amount of breaking area per unit area of surface (Phillips 1985; Kleiss and Melville 2010; Deike et al. 2017a; Deike and Melville 2018), then the mean Lagrangian surface drift (i.e., $z = 0$) of this broken fluid is

$$U_{\mathrm{LB}} = \int u_{\mathrm{LB}} c\mathscr{T}\Lambda(c)\,dc = \alpha\int(\mathscr{S} - \mathscr{S}_0)\frac{c^3}{g}\Lambda(c)\,dc, \quad (6)$$

where we have assumed that the duration of breaking scales with the wave period, that is $\mathscr{T} \sim O(T)$ (Rapp and Melville 1990; Drazen et al. 2008; Deike et al. 2016). Following related scaling arguments (Drazen et al. 2008; Pizzo and Melville 2013), and in the absence of further constraints on this quantity, we take $\mathscr{T} = c/g$. Note, the breaking front has been observed to move at a velocity v below the phase velocity, $0.8c \le v \le c$, which may lead to significant errors in the higher moments. However, a general theoretical description of the speed of the breaking front for various wind and wave conditions is still lacking (Rapp and Melville 1990; Banner and Peirson 2007; Kleiss and Melville 2010; Romero et al. 2012; Banner et al. 2014; Fedele 2014), so here we assume the breaking front moves at speed c (Sutherland and Melville 2013).

Thus, according to this model, the Lagrangian drift due to breaking at the surface is given by the third moment of $\Lambda(c)$, modulated linearly by the slope.

c. Scale-dependent drift

The bulk-scale integrals considered above do not yield information about the scale-dependent drift, or dispersion about the mean. Therefore, we consider the integrands of U_{LB} and U_S and write them in terms of the wavenumber k and phase speed c.

The breaking contribution can be written as

$$U_{\mathrm{LB}} = \int \tilde{u}_{\mathrm{LB}}(c)\,dc, \quad \text{with} \quad \tilde{u}_{\mathrm{LB}} = \alpha(\mathscr{S} - \mathscr{S}_0)\frac{c^3}{g}\Lambda(c), \quad (7)$$

or equivalently in terms of the wavenumber as

$$U_{\mathrm{LB}} = \int \hat{u}_{\mathrm{LB}}(k)\,dk, \quad \text{with}$$
$$\hat{u}_{\mathrm{LB}}(k) = \alpha(\mathscr{S} - \mathscr{S}_0)\frac{g}{2k^3}\Lambda(k), \quad (8)$$

where we have used $\Lambda(c)dc = \Lambda(k)dk$, and the fact that $c^2 = g/k$ and $dk = -2k^{3/2}g^{-1/2}dc$, with the minus sign corresponding to larger c implying smaller k. Note, in the integral for U_{LB}, this minus sign cancels out with the minus sign gained by reversing the direction (from small k to large k) of integration.

The classical Stokes drift integrand at the surface as predicted by Kenyon (1969) is given by

$$U_S = \int \hat{u}_S(k)\,dk, \quad \text{with} \quad \hat{u}_S(k) = 2\phi(k)\sqrt{gk}k, \quad (9)$$

or equivalently in terms of the phase speed as

$$U_S = \int \tilde{u}_S(c)\,dc, \quad \text{with} \quad \tilde{u}_S(c) = 4g^3\phi(c)c^{-6}, \quad (10)$$

where we have used $\phi(c)dc = \phi(k)dk$.

d. Scaling laws for the Stokes drift and breaking drift at the surface

It is of interest to determine the dependence of U_S and U_{LB} on the variables characterizing the wind and wave fields.

To this end, we begin by considering the Stokes drift at the surface U_S and note

$$U_S = 2\int_0^\infty \phi(k)\sqrt{gk}k\,dk = 2\int_0^{k_p} \phi(k)\sqrt{gk}k\,dk + 2\int_{k_p}^{k_n} \phi(k)\sqrt{gk}k\,dk + 2\int_{k_n}^{\infty} \phi(k)\sqrt{gk}k\,dk, \quad (11)$$

where k_p is the peak frequency, and k_n designates the transition wavenumber from the equilibrium to saturation range (Lenain and Melville 2017). Now, following Breivik et al. (2014), we ignore the contribution of the very low wavenumbers as the slopes of these waves are relatively small and hence so is their contribution to the Stokes drift. Next, we let $\phi(k) = \phi_E(k)$ in the equilibrium range $k \in (k_p, k_n)$ and $\phi = \phi_S(k)$ in the saturation range $k \in (k_n, \infty)$. Phillips (1985) proposed, and Lenain and Melville (2017; see also Romero and Melville 2010) have corroborated, that $\phi_E(k) = \beta/2u_*g^{-1/2}k^{-5/2}$ for β a constant and u_* the wind friction velocity. Furthermore, the saturation spectrum is by definition given by $\phi_s = Bk^{-3}$ for B a constant, while k_n is taken to be $k_n = rgu_*^{-2}$ (Phillips 1985; Romero and Melville 2010) for r a scaling

constant taken to be approximately independent of fetch (Lenain and Melville 2017).

Then, the Stokes drift can be shown to scale as

$$U_S = \frac{\beta}{2} u_* \ln\left(\frac{rg}{u_*^2}\frac{1}{k_p}\right) + \frac{2Bu_*}{r^{1/2}}. \tag{12}$$

Finally, we can rewrite this dependence in terms of the phase velocity of the peak component of the spectrum c_p, as $c_p^2 = g/k_p$. Following Sutherland and Melville (2015), we define a spectrally weighted phase velocity c_m, which is a better integral representation of the wind-wave portion of the spectrum (as opposed to c_p, which often characterizes the swell). Sutherland and Melville (2015) found that $c_m \approx 0.7 c_p$.

Equation (12) then becomes

$$\frac{U_S}{u_*} = \frac{\beta}{2} \ln\left(r_2 \frac{c_m^2}{u_*^2}\right) + \frac{2B}{r^{1/2}}, \tag{13}$$

for $r_2 \approx 2r$. Therefore, we expect the (nondimensonalized) Stokes drift to have a weak (logarithmic) dependence on wave age.

Note, these scalings can be used to determine the scalings of the integrand of the Stokes drift in the equilibrium and saturation ranges. To this end, we find

$$\tilde{u}_S = \begin{cases} \dfrac{\beta}{2}\left(\dfrac{c}{u_*}\right)^{-1} & \text{Equilibrium range}, \\ 2B\left(\dfrac{c}{u_*}\right)^{0} & \text{Saturation range}. \end{cases} \tag{14}$$

Next, we repeat this type of argument for the drift induced by breaking, following the recent work of Deike and Melville (2018), based on existing field observations. There, the authors presented a semi-empirical scaling relationship for $\Lambda(c)$, building on the scalings of Sutherland and Melville (2013) and Phillips (1985), while studying gas transfer by breaking waves. In particular, Deike and Melville (2018) proposed that

$$\Lambda(c)\frac{\sqrt{gH_s}^3}{g} = \mu_0 \left(\frac{u_*}{\sqrt{gH_s}}\right)^{5/3} \left(\frac{\sqrt{gH_s}}{c}\right)^6, \tag{15}$$

where $\mu_0 = 0.25 \pm 0.05$ is a scaling constant best fit to the data and the breaking statistics have been scaled by the ballistic velocity $\sqrt{gH_s}$ for H_s the significant wave height. Note, here the nondimensionalization of $\Lambda(c)$ is by $\sqrt{gH_s}$, while in Sutherland and Melville (2013) c_m is used as the velocity scale normalization, with the two variables connected by the fetch relationships. This choice was motivated by laboratory (Drazen et al. 2008), numerical (Deike et al. 2015) and field studies (Romero et al. 2012) on energy dissipation by breaking, that elucidated the role of the ballistic trajectory in setting the scales of the post breaking-induced flow. Furthermore, theoretical (Pizzo and Melville 2013; Pizzo et al. 2016) and numerical (Deike et al. 2016, 2017a) studies have shown the dependence of other bulk scale flow properties (e.g., circulation and volume of air entrained) induced by breaking on the ballistic velocity. Note, in Eq. (15), $\Lambda(c)$ has a c^{-6} dependence which has been shown to be in relative agreement over a range of the existing field data (Kleiss and Melville 2010; Zappa et al. 2012; Sutherland and Melville 2013; Schwendeman et al. 2014; Romero et al. 2017). Next, as in Deike and Melville (2018), and consistent with Romero et al. (2012), we take $\mathcal{S} - \mathcal{S}_0 = A_1(\sqrt{B} - \sqrt{B_T})$, for A_1 a scaling constant and B_T the threshold saturation value for wave breaking, to be a constant which we denote as $\tilde{\mathcal{S}}$. We then find

$$U_{\mathrm{LB}} = \alpha \int_{c_T}^{\infty} (\mathcal{S} - \mathcal{S}_0)\frac{c^3}{g}\Lambda(c)\, dc = \frac{\mu_0 \alpha \tilde{\mathcal{S}}}{2} \frac{u_*^{5/3}\sqrt{gH_S}^{4/3}}{c_T^2}, \tag{16}$$

where c_T is a threshold speed below which waves do not break (Phillips 1985) (which is discussed in more detail below), and we note that the third moment scaling for the drift induced by breaking found here is similar to the scaling found for air and gas entrainment induced by breaking as found in Deike and Melville (2018).

For clarity of presentation, we define

$$\mathcal{U} = \left(u_*^{5/3}\sqrt{gH_S}^{4/3}\right)^{1/3}, \tag{17}$$

so that

$$U_{\mathrm{LB}} = \frac{\mu_0 \alpha \tilde{\mathcal{S}}}{2} \frac{\mathcal{U}^3}{c_T^2}, \tag{18}$$

while the integrand of U_{LB}, that is, $\tilde{u}_{\mathrm{LB}}$, can similarly be shown to scale as

$$\tilde{u}_{\mathrm{LB}} = \mu_0 \alpha \tilde{\mathcal{S}} \left(\frac{\mathcal{U}}{c}\right)^3. \tag{19}$$

Next, the ratio of the scalings of the Stokes drift and the drift induced by breaking is then given by

$$\frac{U_{\mathrm{LB}}}{U_S} = \frac{\mu_0 \alpha \tilde{\mathscr{S}}}{2} \frac{u_*^{2/3} \sqrt{g H_S}^{4/3}}{c_T^2} \frac{1}{\frac{2B}{r^{1/2}} + \frac{\beta}{2} \ln\left(r \frac{c_m^2}{u_*^2}\right)}. \tag{20}$$

The variations in the logarithm are weaker than the polynomial dependence on u_* in the numerator, so we assume this ratio may be approximated as

$$\frac{U_{\mathrm{LB}}}{U_S} \approx \frac{\mu_0 \alpha \tilde{\mathscr{S}}}{2} \frac{u_*^{2/3} \sqrt{g H_S}^{4/3}}{c_T^2} \sim \frac{\mathscr{U}^3}{u_* c_T^2}. \tag{21}$$

We now examine these scaling arguments against the available data.

3. Ocean estimate of drift due to nonbreaking and breaking waves using field measurements

We now examine the predictions of these models using archived field data. Romero et al. (2012), followed by Sutherland and Melville (2013, 2015), showed that to properly close the wave breaking energy budget in the ocean, we need to consider spectral properties of the wave field and compute a spectral breaking parameter $b(c)$, using the wave spectrum (and wave slope spectrum), from high-resolution wave data, together with infrared measurements of the averaged length of breaking crest $\Lambda(c)$ to capture microbreakers that do not entrain a significant amount of air. This was achieved by comparing a measure of the wave energy dissipation using the fifth moment of $\Lambda(c)$, with wave spectral measurements for $b(c)$, to measurements of the subsurface turbulent dissipation due to breaking (Sutherland and Melville 2013, 2015). Building on these studies, we use datasets collected previously and described in earlier publications: infrared video data of $\Lambda(c)$ taken from R/P *FLIP* during the RaDyo 2009, SoCal 2010, and HiRes 2010 experiments (Sutherland and Melville 2013, 2015) combined with measurements of the wave spectrum $\phi(k)$. In Fig. 2, $\Lambda(k)$, $\phi(k)$, and $B(k)$ for the data described above are shown.

Next, as done for air entrainment and gas transfer in Deike and Melville (2018), following Romero et al. (2012), the spatially integrated omnidirectional wave spectrum, $\phi(k)$, is measured in the field, while the saturation spectrum is defined as $B(k) = \phi(k)k^3$. Furthermore, Romero et al.(2012) defined the spectral slope $\mathscr{S} - \mathscr{S}_0$ as $B(k)^{1/2} - B_T^{1/2}$ with a threshold saturation B_T, found to balance wind input and dissipation in a spectral wave model, and consistent with other laboratory (Drazen et al. 2008; Pizzo and Melville 2013), numerical (Deike et al. 2015, 2016),

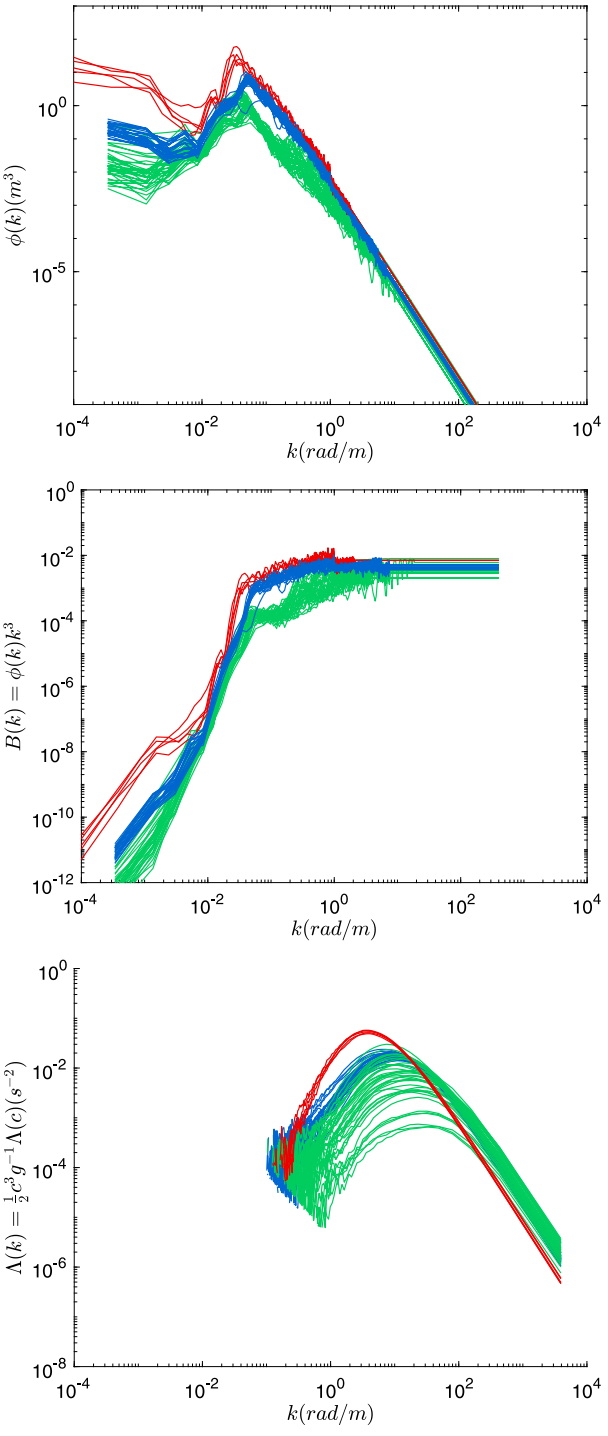

FIG. 2. (top) The azimuth-averaged wave spectrum $\phi(k)$, (middle) the saturation spectrum $B(k)$, and (bottom) the breaking statistic $\Lambda(k)$. Here, green is data from SoCal 2010, blue is data from RaDyo 2009, and red is data from HiRes 2010.

and field experiments (Sutherland and Melville 2013, 2015). The Stokes drift and drift induced by breaking, obtained by integrating Eqs. (9) and (7) using the data

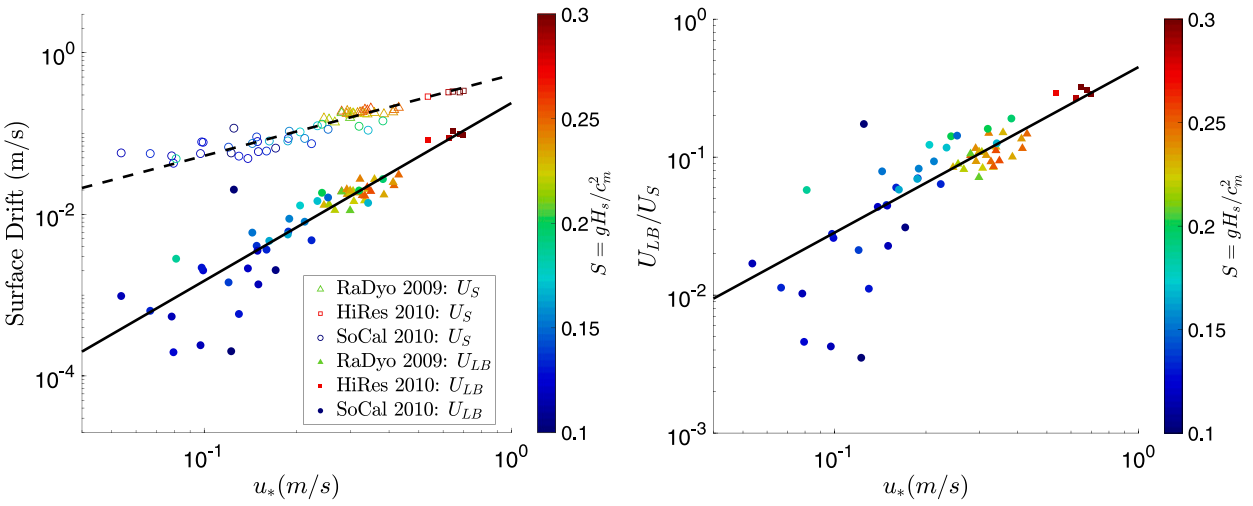

FIG. 3. (left) The Stokes drift U_S (empty symbols) and drift induced by breaking U_{LB} (filled symbols) as a function of u_* for the three datasets considered in this paper. The drift induced by breaking becomes increasingly more important as the wind speed increases, showing a stronger relationship with this variable (solid line) than the Stokes drift (dashed line). The color bar is the ratio of the ballistic velocity squared to the spectrally weighted peak phase velocity squared gH_s/c_m^2 and is a bulk measure of the wave steepness. (right) The ratio of U_{LB} and U_S as a function of u_*.

to compute $\phi(k)$ and $\Lambda(k)$, as a function of wind friction velocity u_* are shown in Fig. 3. The breaking-induced drift shows a stronger relationship with the wind friction velocity than the Stokes drift, with both increasing with u_*. The best fits to the data imply that $U_S = 0.53u_*$, while $U_{\mathrm{LB}} = \kappa_0 u_*^{2.2}$ for $\kappa_0 = 0.24\,(\mathrm{m\ s^{-1}})^{-1.2}$. Note, Wu (1975) found that the wind drift velocity scales as $0.55u_*$, which is close to the relationship found here for the Stokes drift; however, as the wind drift and Stokes drift are two different physical phenomenon, this is merely a coincidence.

We next investigate the scaling models presented in section two, beginning with the scale-dependent drift, to determine the scales at which the Stokes and breaking drift are important. In Fig. 4a we show the integrand of the Stokes drift $\tilde{u}_s$ for the RaDyo 2009 experiment (for clarity of presentation we do not plot all of the data here), as a function of c/u_*. The power law behavior predicted by Eq. (14) is shown by the line in the saturation range [with a $(c/u_*)^0$ dependence] and the line in the equilibrium range [with a $(c/u_*)^{-1}$ dependence], where reasonable agreement between the theoretical predictions and the data is observed. In Fig. 4b, we show the integrand of the breaking-induced Lagrangian drift $\tilde{u}_{\mathrm{LB}}$ as a function of the normalized phase velocity. The scaling arguments given by Eq. (19) imply that breaking-induced drift should scale as c^{-3}, which is in agreement with the data.

Next, we turn to the integrated quantities, that is, the total surface drift. In Fig. 5, the Stokes drift [i.e., Eq. (9)], normalized by the wind friction velocity, is plotted against the reciprocal of the wave age. From the scaling found in section 2, in particular Eq. (13), we expect a weak dependence of the normalized Stokes drift on the wave age, with increasing wave age leading to increasing drift, which is observed in the data presented here.

In Fig. 6, U_{LB} estimated from Eq. (6) is presented. The Lagrangian drift induced by breaking is normalized by the velocity c_T, the threshold phase velocity, below which waves do not break, according to the scaling given by Eq. (16). Following Sutherland and Melville (2013), we take this lower limit to be the point where the spectral Bond number exceeds 10 and the effects of surface tension start to become important (see also the discussion in Deike et al. 2015), which corresponds to $c_T = 0.29\,\mathrm{m\,s^{-1}}$. We see an approximately cubic relationship here between U_{LB}/c_T and $\hat{c}$, where we have defined $\hat{c} = \mathscr{C}/c_T$. Increasing values of S correspond to larger contributions to the breaking-induced drift, as these waves are steeper and hence breaking is more prevalent. The black line shows a cubic fit in $\hat{c}$ to the data, with $U_{\mathrm{LB}}/c_T \approx 0.0013\hat{c}^3$, based on the scaling given in Eq. (18).

Finally, in Fig. 7, we display the ratio U_{LB}/U_S plotted against $\hat{c}$. For the environmental conditions considered here, the breaking-induced drift reaches approximately 30% of the value of the Stokes drift. The relationship is cubic in the variable $\left(\mathscr{C}^3/c_T^2 u_*\right)^{1/3}$, with the drift induced by breaking becoming more significant with increasing wind friction velocity and significant wave height.

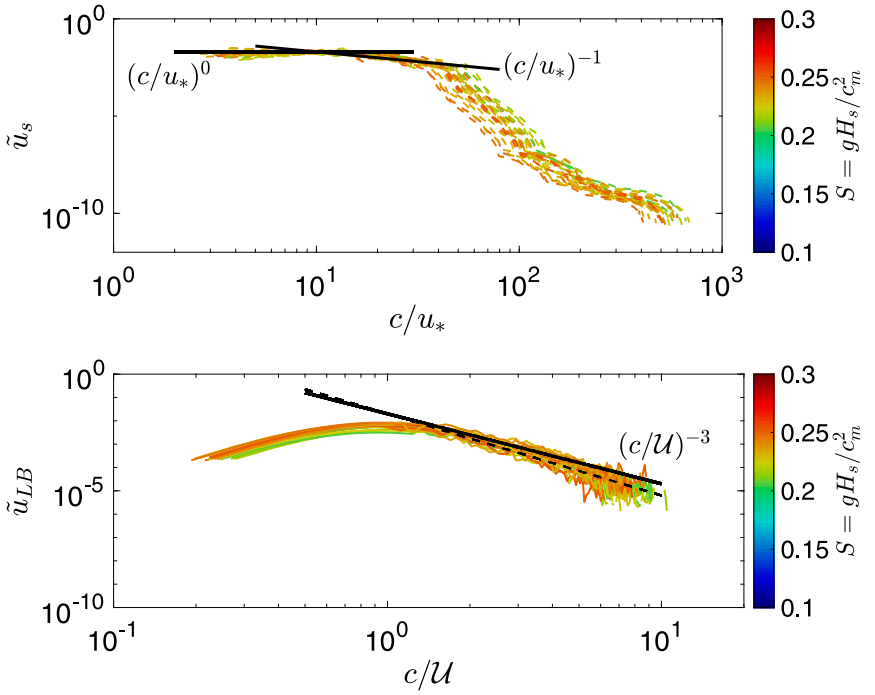

FIG. 4. A plot of (top) $\tilde{u}_S$ and (bottom) $\tilde{u}_{\mathrm{LB}}$, the nonbreaking and breaking components of the wave-induced drift, as a function of c for various values of $S = gH_s/c_m^2$ from the RaDyo 2009 experiments. Note, by Eqs. (8) and (9), $\tilde{u}_S$ and $\tilde{u}_{\mathrm{LB}}$ are nondimensional. The black lines show the scalings proposed in Eqs. (14) and (19), while the dashed line in the bottom plot shows a $(c/\mathscr{U})^{-3.5}$ fit for comparison.

4. Conclusions

The Lagrangian drift induced by wave breaking was studied by extending the model of Deike et al. (2017b) to field data, where the environmental conditions considered have 10 m wind speeds ranging from 1.6 to 16 m s^{-1}, significant wave heights in the range of 0.7–4.7 m and wave ages, here defined as the ratio of the spectrally weighted phase velocity to the wind friction velocity, ranging from 16 to 150. It is found that the drift induced by breaking can be as much as 30% of the classical Stokes drift, and becomes increasingly more important with increasing wind friction velocity and significant wave height.

Note, the turbulent Langmuir number (McWilliams et al. 1997) is defined as $\mathrm{La}_t = \sqrt{u_*^w/U_S}$ for u_*^w the friction velocity in the water (note, this quantity is proportional to the wind friction velocity u_*), which according to our scaling [i.e., Eq. (13)] takes values over [0.18, 0.23], which are in the range of quasi equilibrium conditions (McWilliams et al. 1997; see also Belcher et al. 2012). In the absence of more measurements of these quantities over a broader range of conditions, we leave further discussion to future work.

Next, this paper considers only the mass transport induced at the surface. The depth dependence of this transport is of considerable interest. The laboratory studies of Rapp and Melville (1990), as well as the DNS from Deike et al. (2017b), of deep water breaking waves implies the depth scale of the breaking scales with the height of the

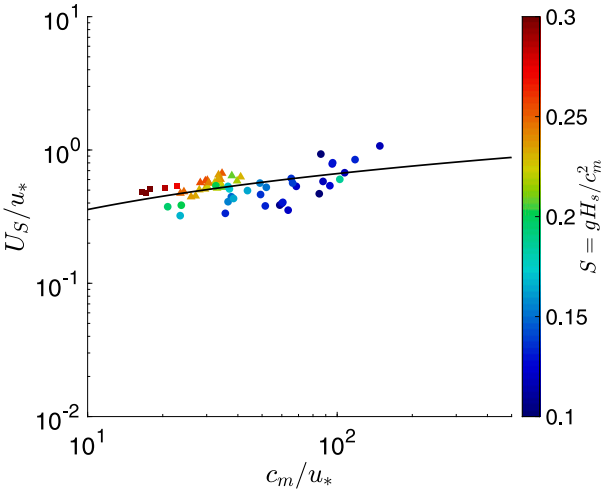

FIG. 5. The Stokes drift, calculated from Eq. (9) as a function of c_m/u_*. The Stokes drift has a weak dependence on wave age, increasing with increasing values of c_m/u_*, in accordance with the scaling given by Eq. (13). The best fit line here has the form $U_S/u_* = 0.13\log(c_m/u_*) + 0.05$.

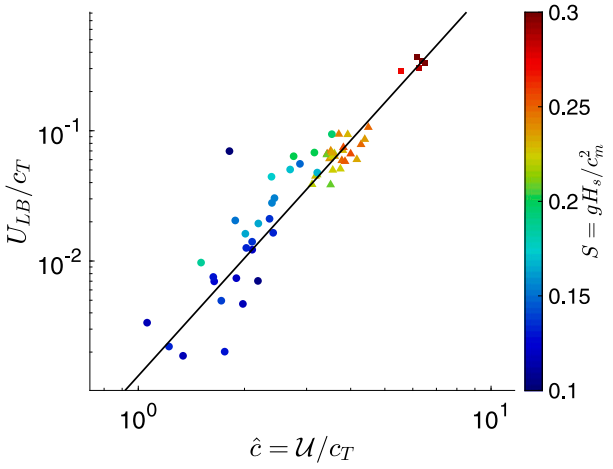

FIG. 6. The Lagrangian drift induced by wave breaking, calculated from Eq. (6) as a function of $\hat{c} = \mathcal{U}/c_T$. The drift increases in magnitude with increasing values of $\hat{c}$, which also corresponds to increasing S. Note, there is more scatter in the data for lower S, as measurements of $\Lambda(c)$ become more difficult due to increased intermittency in the breaking events. The black line shows a cubic fit in $\hat{c}$ to the data, based on the scaling argument given in Eq. (18), with $U_{\mathrm{LB}}/\mathcal{U} \approx 0.0013\hat{c}^3$.

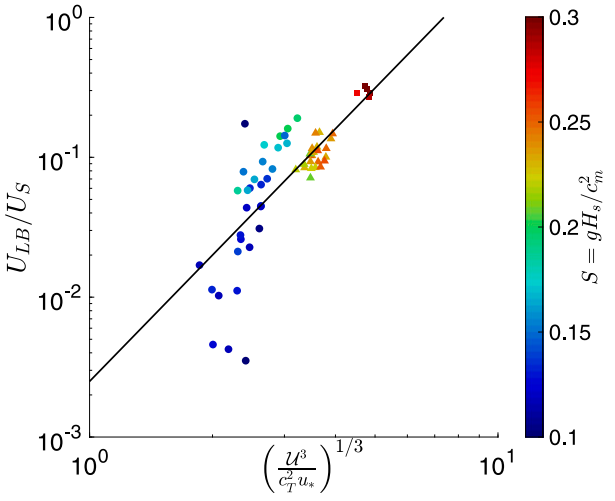

FIG. 7. Ratio of the Lagrangian drift induced by breaking U_{LB} to the Stokes drift U_S, as a function of $\left(\mathcal{U}^3/c_T^2 u_*\right)^{1/3}$. The scaling argument, i.e., Eq. (21), implies that this ratio should increase with the cube of this quantity, which is fit with the black line, with coefficient 0.0025. For the environmental conditions considered here, the drift induced by breaking may be up to 30% of that predicted for the Stokes drift.

wave at breaking. This value may be considerably less than, say, the peak wavenumber used to represent the scale of the depth dependence of the Stokes drift. Further analysis of this depth dependence is in order to better understand the total mass transport due to breaking.

Wave breaking represents an important transfer of momentum flux from the wave field to the water column and must be taken into account for enhanced coupled ocean–atmosphere models. Furthermore, as breaking introduces vorticity into the water column, the dynamics of models including the breaking-induced drift will be markedly different than those without it (Sullivan et al. 2004, 2007). The results presented here should provide bulk scale measures to constrain budgets in coupled ocean–atmosphere models. For example, the breaking statistics of Sutherland and Melville (2013), together with the scaling relationships for the mass transport induced by breaking and nonbreaking waves found here, may be used to close mass, momentum, and energy budgets in coupled LES models of the ocean and atmospheric boundary layers (Sullivan et al. 2007).

Acknowledgments. This research was conducted under grants to W.K.M. from the Office of Naval Research (Grant N00014-17-1-2171) and the National Science Foundation (Physical Oceanography) (Grants NSF 1434198 and OCE-1634289). We thank the referees for comments that have improved the manuscript. N.P. thanks the Kavli Institute for Theoretical Physics at UC Santa Barbara, supported by the National Science Foundation under Grant NSF PHY17-48958, where a portion of this research was conducted. L.D. acknowledges support from the Princeton Environmental Institute at Princeton University and the Cooperative Institute for Climate Sciences between NOAA and Princeton University.

REFERENCES

Banner, M., and W. L. Peirson, 2007: Wave breaking onset and strength for two-dimensional deep-water wave groups. *J. Fluid Mech.*, **585**, 93–115, https://doi.org/10.1017/S0022112007006568.

——, X. Barthelemy, F. Fedele, M. Allis, A. Benetazzo, F. Dias, and W. Peirson, 2014: Linking reduced breaking crest speeds to unsteady nonlinear water wave group behavior. *Phys. Rev. Lett.*, **112**, 114502, https://doi.org/10.1103/PhysRevLett.112.114502.

Belcher, S. E., and Coauthors, 2012: A global perspective on Langmuir turbulence in the ocean surface boundary layer. *Geophys. Res. Lett.*, **39**, L18605, https://doi.org/10.1029/2012GL052932.

Breivik, Ø., P. A. Janssen, and J.-R. Bidlot, 2014: Approximate Stokes drift profiles in deep water. *J. Phys. Oceanogr.*, **44**, 2433–2445, https://doi.org/10.1175/JPO-D-14-0020.1.

Cavaleri, L., B. Fox-Kemper, and M. Hemer, 2012: Wind waves in the coupled climate system. *Bull. Amer. Meteor. Soc.*, **93**, 1651–1661, https://doi.org/10.1175/BAMS-D-11-00170.1.

Craik, A., and S. Leibovich, 1976: A rational model for Langmuir circulations. *J. Fluid Mech.*, **73**, 401–426, https://doi.org/10.1017/S0022112076001420.

Deike, L., and W. Melville, 2018: Gas transfer by breaking waves. *Geophys. Res. Lett.*, **45**, 10 482–10 492, https://doi.org/10.1029/2018GL078758.

——, S. Popinet, and W. K. Melville, 2015: Capillary effects on wave breaking. *J. Fluid Mech.*, **769**, 541–569, https://doi.org/10.1017/jfm.2015.103.

——, W. K. Melville, and S. Popinet, 2016: Air entrainment and bubble statistics in breaking waves. *J. Fluid Mech.*, **801**, 91–129, https://doi.org/10.1017/jfm.2016.372.

——, L. Lenain, and W. K. Melville, 2017a: Air entrainment by breaking waves. *Geophys. Res. Lett.*, **44**, 3779–3787, https://doi.org/10.1002/2017GL072883.

——, N. Pizzo, and W. K. Melville, 2017b: Lagrangian transport by breaking surface waves. *J. Fluid Mech.*, **829**, 364–391, https://doi.org/10.1017/jfm.2017.548.

Donelan, M. A., 1998: Air-water exchange processes. *Physical Processes in Lakes and Oceans*, J. Imberger, Ed., Coastal and Estuarine Studies, Vol. 54, Amer. Geophys. Union, 19–36.

Drazen, D. A., W. K. Melville, and L. Lenain, 2008: Inertial scaling of dissipation in unsteady breaking waves. *J. Fluid Mech.*, **611**, 307–332, https://doi.org/10.1017/S0022112008002826.

Fedele, F., 2014: Geometric phases of water waves. *EPL*, **107**, 69001, https://doi.org/10.1209/0295-5075/107/69001.

Grue, J., and J. Kolaas, 2017: Experimental particle paths and drift velocity in steep waves at finite water depth. *J. Fluid Mech.*, **810**, R1, https://doi.org/10.1017/jfm.2016.726.

John, F., 1953: Two-dimensional potential flows with a free boundary. *Commun. Pure Appl. Math.*, **6**, 497–503, https://doi.org/10.1002/cpa.3160060405.

Kenyon, K. E., 1969: Stokes drift for random gravity waves. *J. Geophys. Res.*, **74**, 6991–6994, https://doi.org/10.1029/JC074i028p06991.

Kleiss, J. M., and W. K. Melville, 2010: Observations of wave breaking kinematics in fetch-limited seas. *J. Phys. Oceanogr.*, **40**, 2575–2604, https://doi.org/10.1175/2010JPO4383.1.

Leibovich, S., 1983: The form and dynamics of Langmuir circulations. *Annu. Rev. Fluid Mech.*, **15**, 391–427, https://doi.org/10.1146/annurev.fl.15.010183.002135.

Lenain, L., and W. K. Melville, 2017: Measurements of the directional spectrum across the equilibrium saturation ranges of wind-generated surface waves. *J. Phys. Oceanogr.*, **47**, 2123–2138, https://doi.org/10.1175/JPO-D-17-0017.1.

McWilliams, J. C., and J. M. Restrepo, 1999: The wave-driven ocean circulation. *J. Phys. Oceanogr.*, **29**, 2523–2540, https://doi.org/10.1175/1520-0485(1999)029<2523:TWDOC>2.0.CO;2.

——, P. P. Sullivan, and C.-H. Moeng, 1997: Langmuir turbulence in the ocean. *J. Fluid Mech.*, **334**, 1–30, https://doi.org/10.1017/S0022112096004375.

Melville, W. K., 1994: Energy dissipation by breaking waves. *J. Phys. Oceanogr.*, **24**, 2041–2049, https://doi.org/10.1175/1520-0485(1994)024<2041:EDBBW>2.0.CO;2.

——, R. Shear, and F. Veron, 1998: Laboratory measurements of the generation and evolution of Langmuir circulations. *J. Fluid Mech.*, **364**, 31–58, https://doi.org/10.1017/S0022112098001098.

Mueller, J. A., and F. Veron, 2009: Nonlinear formulation of the bulk surface stress over breaking waves: Feedback mechanisms from air-flow separation. *Bound.-Layer Meteor.*, **130**, 117, https://doi.org/10.1007/s10546-008-9334-6.

Phillips, O., 1985: Spectral and statistical properties of the equilibrium range in wind-generated gravity waves. *J. Fluid Mech.*, **156**, 505–531, https://doi.org/10.1017/S0022112085002221.

Pizzo, N., 2017: Surfing surface gravity waves. *J. Fluid Mech.*, **823**, 316–328, https://doi.org/10.1017/jfm.2017.314.

——, and W. K. Melville, 2013: Vortex generation by deep-water breaking waves. *J. Fluid Mech.*, **734**, 198–218, https://doi.org/10.1017/jfm.2013.453.

——, ——, and L. Deike, 2016: Current generation by deep-water wave breaking. *J. Fluid Mech.*, **803**, 292–312, https://doi.org/10.1017/jfm.2016.473.

Rapp, R., and W. Melville, 1990: Laboratory measurements of deep-water breaking waves. *Philos. Trans. Roy. Soc. London*, **331A**, 735–800, https://doi.org/10.1098/rsta.1990.0098.

Romero, L., and W. K. Melville, 2010: Airborne observations of fetch-limited waves in the Gulf of Tehuantepec. *J. Phys. Oceanogr.*, **40**, 441–465, https://doi.org/10.1175/2009JPO4127.1.

——, ——, and J. M. Kleiss, 2012: Spectral energy dissipation due to surface wave breaking. *J. Phys. Oceanogr.*, **42**, 1421–1444, https://doi.org/10.1175/JPO-D-11-072.1.

——, L. Lenain, and W. K. Melville, 2017: Observations of surface wave–current interaction. *J. Phys. Oceanogr.*, **47**, 615–632, https://doi.org/10.1175/JPO-D-16-0108.1.

Schwendeman, M., J. Thomson, and J. R. Gemmrich, 2014: Wave breaking dissipation in a young wind sea. *J. Phys. Oceanogr.*, **44**, 104–127, https://doi.org/10.1175/JPO-D-12-0237.1.

Sullivan, P. P., J. C. McWilliams, and W. K. Melville, 2004: The oceanic boundary layer driven by wave breaking with stochastic variability. Part 1. Direct numerical simulations. *J. Fluid Mech.*, **507**, 143–174, https://doi.org/10.1017/S0022112004008882.

——, ——, and ——, 2007: Surface gravity wave effects in the oceanic boundary layer: Large-eddy simulation with vortex force and stochastic breakers. *J. Fluid Mech.*, **593**, 405–452, https://doi.org/10.1017/S002211200700897X.

Sutherland, P., and W. K. Melville, 2013: Field measurements and scaling of ocean surface wave breaking statistics. *Geophys. Res. Lett.*, **40**, 3074–3079, https://doi.org/10.1002/grl.50584.

——, and ——, 2015: Field measurements of surface and near-surface turbulence in the presence of breaking waves. *J. Phys. Oceanogr.*, **45**, 943–965, https://doi.org/10.1175/JPO-D-14-0133.1.

Suzuki, N., and B. Fox-Kemper, 2016: Understanding stokes forces in the wave-averaged equations. *J. Geophys. Res. Oceans*, **121**, 3579–3596, https://doi.org/10.1002/2015JC011566.

Terray, E., M. Donelan, Y. Agrawal, W. Drennan, K. Kahma, A. J. Williams, P. Hwang, and S. Kitaigorodskii, 1996: Estimates of kinetic energy dissipation under breaking waves. *J. Phys. Oceanogr.*, **26**, 792–807, https://doi.org/10.1175/1520-0485(1996)026<0792:EOKEDU>2.0.CO;2.

van den Bremer, T., and P. Taylor, 2016: Lagrangian transport for two-dimensional deep-water surface gravity wave groups. *Proc. Roy. Soc. London*, **472A**, 20160159, https://doi.org/10.1098/rspa.2016.0159.

——, and Ø. Breivik, 2018: Stokes drift. *Philos. Trans. Roy. Soc. London*, **376A**, 20170104, https://doi.org/10.1098/rsta.2017.0104.

Veron, F., and W. K. Melville, 2001: Experiments on the stability and transition of wind-driven water surfaces. *J. Fluid Mech.*, **446**, 25–65.

Wu, J., 1975: Wind-induced drift currents. *J. Fluid Mech.*, **68**, 49–70, https://doi.org/10.1017/S0022112075000687.

——, 1982: Wind-stress coefficients over sea surface from breeze to hurricane. *J. Geophys. Res.*, **87**, 9704–9706, https://doi.org/10.1029/JC087iC12p09704.

Zappa, C. J., M. L. Banner, H. Schultz, J. R. Gemmrich, R. P. Morison, D. A. LeBel, and T. Dickey, 2012: An overview of sea state conditions and air-sea fluxes during RaDyO. *J. Geophys. Res.*, **117**, C00H19, https://doi.org/10.1029/2011JC007336.